THE JOURNAL OF BIOLOGICAL CHEMISTRY VOL. 289, NO. 40, pp. 27456–27468, October 3, 2014

Multiple Propofol-binding Sites in a γ-Aminobutyric Acid Type A Receptor ($GABA_AR$) Identified Using a Photoreactive Propofol Analog*◆

Received for publication, May 14, 2014, and in revised form, July 30, 2014 Published, JBC Papers in Press, August 1, 2014, DOI 10.1074/jbc.M114.581728

Selwyn S. Jayakar[‡], Xiaojuan Zhou[§], David C. Chiara[‡], Zuzana Dostalova[§], Pavel Y. Savechenkov[¶], Karol S. Bruzik[¶], William P. Dailey[‖], Keith W. Miller[§], Roderic G. Eckenhoff[‡‡], and Jonathan B. Cohen[‡1]**

*From the Departments of [‡]Neurobiology and **Biological Chemistry and Molecular Pharmacology, Harvard Medical School, Boston, Massachusetts 02115, the [§]Department of Anesthesia, Critical Care and Pain Medicine, Massachusetts General Hospital, Boston, Massachusetts 02114, the [¶]Department of Medicinal Chemistry and Pharmacognosy, University of Illinois at Chicago, Chicago, Illinois 60612, and the [‖]Department of Chemistry, University of Pennsylvania and [‡‡]Department of Anesthesiology and Critical Care, University of Pennsylvania Perelman School of Medicine, Philadelphia, Pennsylvania 19104*

Background: Propofol binding to $GABA_AR$ sites of uncertain location potentiates receptor function and produces anesthesia *in vivo*.
Results: A photoreactive propofol analog identifies propofol-binding sites in $\alpha1\beta3$ $GABA_ARs$.
Conclusion: Propofol binds to each class of intersubunit sites in the $GABA_AR$ transmembrane domain.
Significance: This study demonstrates that propofol binds to the same sites in a $GABA_AR$ as etomidate and barbiturates.

Propofol acts as a positive allosteric modulator of γ-aminobutyric acid type A receptors ($GABA_ARs$), an interaction necessary for its anesthetic potency *in vivo* as a general anesthetic. Identifying the location of propofol-binding sites is necessary to understand its mechanism of $GABA_AR$ modulation. [^{3}H]2-(3-Methyl-3*H*-diaziren-3-yl)ethyl 1-(phenylethyl)-1*H*-imidazole-5-carboxylate (azietomidate) and *R*-[^{3}H]5-allyl-1-methyl-5-(*m*-trifluoromethyl-diazirynylphenyl)barbituric acid (*m*TFD-MPAB), photoreactive analogs of 2-ethyl 1-(phenylethyl)-1*H*-imidazole-5-carboxylate (etomidate) and mephobarbital, respectively, have identified two homologous but pharmacologically distinct classes of intersubunit-binding sites for general anesthetics in the $GABA_AR$ transmembrane domain. Here, we use a photoreactive analog of propofol (2-isopropyl-5-[3-(trifluoromethyl)-3*H*-diazirin-3-yl]phenol ([^{3}H]AziP*m*)) to identify propofol-binding sites in heterologously expressed human $\alpha1\beta3$ $GABA_ARs$. Propofol, AziP*m*, etomidate, and *R*-*m*TFD-MPAB each inhibited [^{3}H]AziP*m* photoincorporation into $GABA_AR$ subunits maximally by ~50%. When the amino acids photolabeled by [^{3}H]AziP*m* were identified by protein microsequencing, we found propofol-inhibitable photolabeling of amino acids in the $\beta3$-$\alpha1$ subunit interface (β3Met-286 in β3M3 and α1Met-236 in α1M1), previously photolabeled by [^{3}H]azietomidate, and α1Ile-239, located one helical turn below α1Met-236. There was also propofol-inhibitable [^{3}H]AziP*m* photolabeling of β3Met-227 in βM1, the amino acid in the $\alpha1$-$\beta3$ subunit interface photolabeled by *R*-[^{3}H]*m*TFD-MPAB. The propofol-inhibitable [^{3}H]AziP*m* photolabeling in the $GABA_AR$ $\beta3$ subunit in conjunction with the concentration dependence of inhibition of that photolabeling by etomidate or *R*-*m*TFD-MPAB also establish that each anesthetic binds to the homologous site at the $\beta3$-$\beta3$ subunit interface. These results establish that AziP*m* as well as propofol bind to the homologous intersubunit sites in the $GABA_AR$ transmembrane domain that binds etomidate or *R*-*m*TFD-MPAB with high affinity.

Propofol, a widely used intravenous general anesthetic, acts as a positive allosteric modulator of inhibitory GABA type A receptors ($GABA_AR$),[2] an interaction that determines its anesthetic potency *in vivo* (1–4). However, the number and location of $GABA_AR$-binding sites for propofol remain uncertain. $GABA_ARs$ are members of the superfamily of pentameric ligand-gated ion channels formed by five identical or homologous subunits that associate around a central axis that forms the ion channel (5, 6). Each subunit is made up of an N-terminal extracellular domain, a transmembrane domain (TMD) formed by a loose bundle of four transmembrane helices (M1–M4), with amino acids on one face of each M2 helix contributing to the lumen of the ion channel, and an intracellular domain formed by the amino acids between the M3 and M4 helices.

$GABA_AR$ residues that may contribute to propofol-binding sites, identified by analyses of the functional properties of mutant receptors, include positions 15 of the β subunit M2

* This work was supported, in whole or in part, by National Institutes of Health Grants GM-58448 (to J. B. C., K. S. B., and K. W. M.) and GM-55876 (to R. G. E.) from USPHS.
◆ This article was selected as a Paper of the Week.
[1] To whom correspondence should be addressed: Dept. of Neurobiology, Harvard Medical School, 220 Longwood Ave., Boston, MA 02115. Tel.: 617-432-1728; Fax: 617-432-1639; E-mail: jonathan_cohen@hms.harvard.edu.

[2] The abbreviations used are: $GABA_AR$, γ-aminobutyric acid type A receptor; AziP*m*, 2-isopropyl-5-[3-(trifluoromethyl)-3*H*-diazirin-3-yl]phenol; *o*-PD, *o*-propofol diazirine; azietomidate, 2-(3-methyl-3*H*-diaziren-3-yl)ethyl 1-(phenylethyl)-1*H*-imidazole-5-carboxylate; etomidate, 2-ethyl 1-(phenylethyl)-1*H*-imidazole-5-carboxylate; TDBzl-etomidate, 4-[3-(trifluoromethyl)-3*H*-diazirin-3-yl]benzyl-1-(1-phenylethyl)-1*H*-imidazole-5-carboxylate; *m*TFD-MPAB, 5-allyl-1-methyl-5-(*m*-trifluoromethyl-diazirynylphenyl)barbituric acid; nAChR, nicotinic acetylcholine receptor; TMD, transmembrane domain; EndoGlu-C, *S. aureus* endopeptidase Glu-C; EndoLys-C, *L. enzymogenes* endoproteinase Lys-C; rpHPLC, reversed-phase high pressure liquid chromatography; OPA, *o*-phthalaldehyde; BNPS-skatole, 3-bromo-3-methyl-2-(2-nitrophenylthio)-3*H*-indole; PPF, propofol; PTH, phenylthiohydantoin.

helix (βM2–15′) and four of the M3 helix (βM3–4′, β3Met-286), numbered relative to the conserved Arg and Asp near the N terminus of each subunit's M2 and M3 helices, respectively (7, 8). In addition, positions in βM4 (9) and in the α subunit cytoplasmic domain (10) have been identified as propofol sensitivity determinants. These propofol sensitivity determinants can be located in models of heteromeric GABA$_A$Rs constructed by homology from the recently solved structure of a homomeric β3 GABA$_A$R (11) or the structures of other pentameric ligand-gated ion channels, including the *Torpedo* nicotinic acetylcholine receptor (nAChR) (12), the prokaryotic proton-gated channel GLIC (13), the amine-gated channel ELIC (14), and the invertebrate glutamate-gated channel GluCl (15). In these models, βM2–15′ and βM3–4′, positions that are also sensitivity determinants for the intravenous anesthetic etomidate, are present in a pocket at the interface between the β and α subunits that contains the transmitter-binding sites in the extracellular domain (referred to as the β^+-α^- interface) (16, 17), although the other sensitivity determinants are not within that intersubunit pocket. That etomidate binds to this intersubunit site was established by the etomidate-inhibitable photoincorporation of reactive etomidate analogs into βM3–4′ and α1Met-236 in αM1 in a heterogeneous population of GABA$_A$Rs purified from bovine brain (18) and in purified human $\alpha1\beta3$ GABA$_A$R (16).

Recently, photoaffinity labeling studies with *R*-[^{3}H]*m*TFD-MPAB, a photoreactive barbiturate, identified a second class of general anesthetic-binding sites in human $\alpha1\beta3\gamma2$ GABA$_A$Rs at the β^--α^+ and β^--γ^+ subunit interfaces (19). Although etomidate bound selectively to the β^+ interface sites and certain barbiturates bound selectively at the β^- interface sites, propofol inhibited photolabeling at both classes of sites, but only at concentrations (IC_{50} ~40 μM) that were ~10-fold higher than the concentrations necessary to potentiate GABA responses. This discrepancy suggests that propofol may bind with higher affinity to other, as yet unidentified, sites in the GABA$_A$R. A reactive propofol analog (*o*-propofol diazirine (*o*-PD)) was recently shown to photoincorporate in expressed $\alpha1\beta3$ GABA$_A$R into β3His-267 (βM2–17′), an amino acid in the β subunit M2 helix in proximity to the *R*-*m*TFD-MPAB site, but projecting into the lumen of the ion channel near the interface between the extracellular and transmembrane domains (20).

In this report, we identify propofol-binding sites in a purified human $\alpha1\beta3$ GABA$_A$R using 2-isopropyl-5-[3-(trifluoromethyl)-3*H*-diazirin-3-yl]phenol (AziP*m*), a photoreactive propofol analog that potentiates GABA responses and acts as a general anesthetic (Fig. 1) (21). Propofol and AziP*m* are nAChR inhibitors, and photoaffinity labeling of the *Torpedo* nAChR established propofol-inhibitable photoincorporation of [^{3}H]AziP*m* into two sites in the TMD as follows: an intrasubunit site in the δ subunit helix bundle, and a site in the ion channel (22). Propofol and AziP*m* are also inhibitors of GLIC, and in GLIC crystals propofol binds in the TMD in the intrasubunit pocket formed by the four transmembrane helices (23). In purified GLIC in detergent solution, propofol inhibited [^{3}H]AziP*m* photolabeling of amino acids in that binding pocket (24). Based upon the identification of the GABA$_A$R amino acids photolabeled by [^{3}H]AziP*m* and the effects of propofol, AziP*m*, and *o*-PD on GABA$_A$R photolabeling by [^{3}H]azietomidate and *R*-[^{3}H]*m*TFD-MPAB, we found in this study that propofol, AziP*m*, and *o*-PD bind in the $\alpha1\beta3$ GABA$_A$R to the same intersubunit sites as etomidate and *R*-*m*TFD-MPAB, *i.e.* the homologous sites at the β^+-α^-, α^+-β^-, and β^+-β^- subunit interfaces. We found no evidence of [^{3}H]AziP*m* photolabeling of GABA$_A$R amino acids that would be located in intrasubunit binding pockets or in the ion channel.

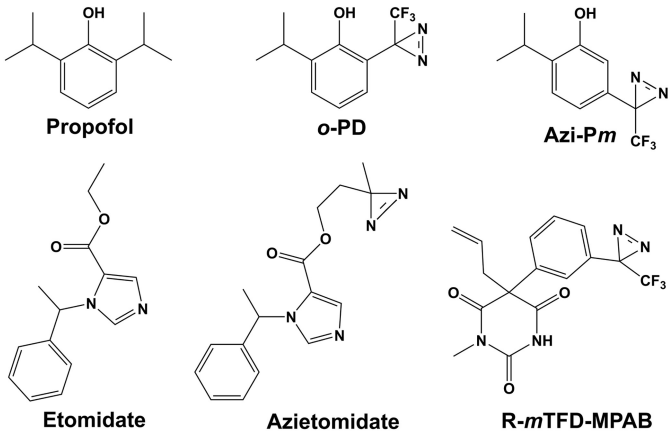

FIGURE 1. **Structures of propofol, etomidate, and photoreactive general anesthetics.**

EXPERIMENTAL PROCEDURES

Materials—Nonradioactive AziP*m* was synthesized as described (21), and [^{3}H]AziP*m* (10 Ci/mmol) was prepared by AmBios (Newington, CT) by ring iodination followed by catalytic reduction with tritium gas. Nonradioactive *R*-*m*TFD-MPAB and *R*-[^{3}H]*m*TFD -MPAB (38 Ci/mmol) were prepared previously (25), as was [^{3}H]azietomidate (12 Ci/mmol) (26), which was also resynthesized at 19 Ci/mmol by catalytic reduction of *m*-bromoazietomidate with tritium gas. *o*-PD was synthesized from 2-isopropyl-6-trifluoroacetylphenol as described (20) with the purity >96% as judged by ^{1}H and ^{19}F NMR. As reported (20), the UV spectrum was characterized by an absorption maximum at 280 nm (extinction coefficient, ϵ_{280} = 2417 ± 24 M^{-1} cm^{-1}) and an unresolved long wavelength shoulder (ϵ_{350} = 66 ± 1 M^{-1} cm^{-1}), and when stored in ethanol at −20 °C, *o*-PD was stable for more than 1 month. *n*-Dodecyl-β-D-maltopyranoside, sodium cholate, and CHAPS were from Anatrace-Affymetrix (Anagrade quality). (*R*)-Etomidate was from Organon Laboratories. Soybean asolectin, FLAG peptide (DYKDDDDK), γ-aminobutyric acid (GABA), propofol, 3-bromo-3-methyl-2-(2-nitrophenylthio)-*3H*-indole (BNPS-skatole), and cyanogen bromide (CNBr) were from Sigma. *o*-Phthalaldehyde (OPA) was from Alfa Aesar. *Lysobacter enzymogenes* lysine-C endopeptidase (EndoLys-C) was from Roche Applied Science, and *Staphylococcus aureus* glutamic-C endopeptidase (EndoGlu-C) was from Princeton Separations.

Purification of Expressed $\alpha1\beta3$ GABA$_A$Rs—$\alpha1\beta3$ GABA$_A$Rs containing the FLAG epitope at the N terminus of the $\alpha1$ subunit were purified from a tetracycline-inducible, stably transfected HEK293S cell line (27). Briefly, membrane fractions containing 6–10 nmol of [^{3}H]muscimol-binding sites, collected from cells growing on 40–60 tissue culture dishes (15 cm), were resuspended at 1 mg of protein/ml and solubilized overnight in

300 ml of a purification buffer (50 mM Tris-HCl (pH 7.4), 150 mM NaCl, 2 mM $CaCl_2$, 5 mM KCl, 5 mM $MgCl_2$, 4 mM EDTA, 20% glycerol, pepstatin, chymostatin, and leupeptin (10 μg/ml each), 2 μg/ml aprotinin, and 1 mM phenylmethanesulfonyl fluoride) supplemented with 2.5 mM *n*-dodecyl-β-D-maltopyranoside. Solubilized FLAG-$\alpha1\beta3$ $GABA_ARs$ were purified by elution from an anti-FLAG M2 affinity resin in elution buffer (purification buffer supplemented with 11.5 mM cholate, 0.86 mM asolectin, and 1.5 mM FLAG peptide). For competition photolabeling studies, $GABA_AR$ was also purified by solubilization for 2.5 h in purification buffer supplemented with 30 mM *n*-dodecyl-β-D-maltopyranoside followed by elution from the anti-FLAG affinity resin after washing in purification buffer supplemented with 5 mM CHAPS and 0.2 mM asolectin, as described for the $\alpha1\beta3\gamma2$ $GABA_AR$ (19). For both protocols, typical purification yields were ~1.5 nmol of purified receptor (50–60 nM binding sites) in 15–25 ml of elution buffer. For the $GABA_AR$ purified in 0.86 mM asolectin, 11.5 mM cholate, IC_{50} values (total concentration) for inhibition of [^{3}H]azietomidate, *R*-[^{3}H]*m*TFD-MPAB, or [^{3}H]AziP*m* photolabeling were 2–4-fold higher than for $GABA_AR$ purified in 0.2 mM asolectin, 5 mM CHAPS.

Photoaffinity Labeling—Aliquots of FLAG-$\alpha1\beta3$ $GABA_ARs$ in elution buffer were used for analytical and preparative scale photolabeling (40–80 μl and 1 ml of $\alpha1\beta3$ $GABA_AR$, per condition, respectively). Appropriate volumes of radiolabeled, photoreactive anesthetic solutions in methanol were transferred to glass tubes, and solvent was evaporated under an argon stream. Freshly thawed $GABA_AR$ in elution buffer was added to the tube, and radioligand was resuspended with gentle vortexing during 30 min on ice to a final [^{3}H]AziP*m* concentration of ~5 μM (2.5 μCi per condition) for analytical or ~10 μM (90 μCi per condition) for preparative scale experiments. $GABA_AR$ was equilibrated with [^{3}H]azietomidate or *R*-[^{3}H]*m*TFD-MPAB at final concentrations of 0.9 or 1.5 μM, respectively. Receptors were then equilibrated for 10 min with 1 mM GABA before addition of appropriate concentrations of nonradioactive anesthetic. After further incubation on ice for 30 min, the aliquots were transferred to 96-well plastic plates (Corning catalog number 2797) or 3.5-cm diameter plastic Petri dishes (Corning catalog number 3001) for analytical or preparative photolabelings, respectively, and irradiated on ice for 30 min at a distance of 0.5 to 1 cm with a 365 nm lamp (Spectroline Model EN-16, Spectronics Corp, Westbury, NJ). Stock solutions of nonradioactive AziP*m* (200 mM), propofol (1 M), *R*-*m*TFD-MPAB (60 mM), and etomidate (60 mM) were prepared in methanol, and all samples were photolabeled at a methanol concentration of 0.5% (v/v).

SDS-PAGE and Subunit Fragmentation—Following irradiation, samples were mixed with an equal volume of electrophoresis sample buffer (16), incubated for 30–60 min at room temperature, and then fractionated by SDS-PAGE on a 6% Tris-glycine gel. For analytical scale labeling, samples were loaded onto wells 2 cm deep, 0.8 cm wide, and 0.15 cm thick (sample volume, 150 μl). Preparative scale labeling samples were loaded onto wells 2 cm deep, 11.3 cm wide, and 0.15-cm thick (sample volume, 1.5 ml). Subunits resolved by SDS-PAGE were visualized by Coomassie Brilliant Blue stain and excised to measure incorporated ^{3}H (for analytical scale experiments) or eluted and digested to generate peptide fragments for sequence analysis. For analytical scale experiments, the excised subunits were incubated overnight with 200 μl of deionized water and 500 μl of TS-2 tissue solubilizer (Research Products), and then ^{3}H incorporation was determined by liquid scintillation counting after adding 5 ml of Ecoscint A (National Diagnostics).

After photolabeling on a preparative scale, $GABA_AR$ subunits were recovered from the excised gel bands as described (16) and resuspended in 200 μl of digestion buffer (15 mM Tris, 500 μM EDTA, and 0.1% SDS (pH 8.5)). Aliquots (~90 μl) from gel bands enriched in $\alpha1$ or $\beta3$ subunits were digested at room temperature with 0.5 units of EndoLys-C for 14 days or 2.5 μg of EndoGlu-C for 2–4 days, following which the digests were fractionated by HPLC or directly subjected to protein microsequence analysis. For chemical cleavage at the C terminus of methionines, samples immobilized on PVDF sequencing filters were treated with cyanogen bromide as described (28, 29). For chemical cleavage at the C terminus of tryptophans, samples on PVDF filters were treated with BNPS-skatole as described (30), except that after precipitation of excess BNPS-skatole, the digestion solution was loaded onto a second PVDF filter, and material on the two filters was sequenced simultaneously (16). $\alpha1\beta3$ $GABA_AR$ amino acids photolabeled by *R*-[^{3}H]*m*TFD-MPAB were identified as described for the $\alpha1\beta3\gamma2$ $GABA_AR$ (19).

Quantification of Anesthetic Inhibition of $GABA_AR$ Photolabeling—The concentration dependence of inhibition of ^{3}H incorporation into $GABA_AR$ subunits was fit by nonlinear least squares using SigmaPlot to a single site model, Equation 1,

$$f(x) = (f_0 - f_{ns})/(1 + x/IC_{50}) + f_{ns} \quad \text{(Eq. 1)}$$

where $f(x)$ is the ^{3}H counts/min (cpm) incorporated into a subunit at the inhibitor total concentration x; f_0 is the subunit ^{3}H in the absence of inhibitor; IC_{50} is the total inhibitor concentration reducing photolabeling by 50%, and f_{ns} is the nonspecific subunit photolabeling. IC_{50} was the adjustable parameter. For [^{3}H]azietomidate and *R*-[^{3}H]*m*TFD-MPAB, f_{ns} was the residual subunit photolabeling in the presence of 300 μM etomidate or 2.5 mM pentobarbital, respectively. For [^{3}H]AziP*m* the f_{ns} was determined in the presence of either 300 μM etomidate or *R*-*m*TFD-MPAB. Although ^{3}H incorporation was determined separately for the three gel bands, IC_{50} values were determined for inhibition of [^{3}H]azietomidate photoincorporation in the ~56-kDa α subunit band that reflects photolabeling of α1Met-236 and for *R*-[^{3}H]*m*TFD-MPAB (16) in the 59- and 61-kDa β subunit bands that reflect photolabeling of β3Met-227 (see under "Results"). For [^{3}H]AziP*m*, inhibition of photolabeling was quantified only for the β subunit bands, as pharmacologically specific photolabeling was too small a component of α subunit photolabeling. For $GABA_AR$ purified in 0.2 mM asolectin, 5 mM CHAPS, photolabeling in the presence of nonradioactive AziP*m* at concentrations >30 μM resulted in $GABA_AR$ aggregation, as evidenced by decreased stain intensity of $GABA_AR$ subunit gel bands after SDS-PAGE. IC_{50} values for AziP*m* were determined from data at concentrations ≤30 μM.

Reversed-phase HPLC and Sequence Analysis—Subunit fragments generated by enzymatic digestion were fractionated by

reversed phase HPLC (rpHPLC) on an Agilent 1100 binary HPLC system, using a Brownlee C4-Aquapore column (100 × 2.1 mm, 7 μ particle size) at 40 °C. Solvent A was 0.08% trifluoroacetic acid in water, and solvent B was 0.05% trifluoroacetic acid in 60% acetonitrile and 40% 2-propanol. A nonlinear elution gradient increasing from 5 to 100% solvent B in 80 min was used at a flow rate of 200 μl/min, with 0.5-ml fractions collected. ^{3}H distribution was determined by counting aliquots (10%) of each fraction, and peptide elution was monitored by absorbance at 215 nm. The rpHPLC fractions containing peaks of ^{3}H were pooled and drop-loaded at 45 °C onto Micro TFA glass fiber filters (Applied Biosystems). Digests of intact $GABA_AR$ subunits and selected rpHPLC fractions were loaded directly onto PVDF filters using Prosorb (Applied Biosystems) sample preparation cartridges. All filters were treated after loading with Biobrene (Applied Biosystems) before sequencing.

Samples were sequenced using a Procise 492 protein sequencer (Applied Biosystems) programmed to use ⅔ of the material from each cycle of Edman degradation for PTH-derivative quantification and ⅓ to measure the ^{3}H release by scintillation counting. For some samples, sequencing was interrupted at designated cycles, and the sample filter was treated with OPA to chemically isolate for further sequencing only those fragments containing a proline in the designated cycle. OPA reacts with primary amines, but not secondary amines, and treatment with OPA blocks further sequencing of any fragment not containing a proline at that cycle (31, 32). The amount of PTH-derivative released (in picomoles) for a given residue was quantified using their peak height in the chromatogram, background-corrected, compared with a standard peak, and fit by nonlinear least squares to Equation 2,

$$I_x = I_0 R^x \qquad \text{(Eq. 2)}$$

where I_x is the mass of the peptide residue in cycle x (in picomoles); I_0 is the initial amount of peptide (in picomoles), and R is the average repetitive yield. Amino acid derivatives whose amounts could not be accurately estimated (His, Trp, Ser, Arg, and Cys) were omitted from the fit. The efficiency of photolabeling (in cpm/pmol) for a given amino acid residue was calculated by Equation 3,

$$E(x) = 2 \times (\text{cpm}_x - \text{cpm}_{(x-1)})/(I_0 \times R^x) \qquad \text{(Eq. 3)}$$

where cpm_x is the ^{3}H released in cycle $\boldsymbol{x}$.

Molecular Modeling—The Discovery studio 2.5.5 molecular modeling package (Accelrys, Inc.) was used as described (19) to dock propofol, AziP*m*, and *o*-PD in potential anesthetic binding pockets in two homology models of a human $\alpha1\beta3$ $GABA_AR$ with a $\beta3$-$\alpha1$-$\beta3$-$\alpha1$-$\beta3$ subunit order as follows: (i) a model described previously (16) derived from the crystal structure of GLIC (Protein Data Bank code 3P50); and (ii) a model based upon the recently published structure of a human homopentameric $\beta3$ $GABA_AR$ ((Protein Data Bank code 4COF (11)). This new model was created by replacing the $\beta3$ sequences of the subunits designated A and C with the human $\alpha1$ sequence, an alignment requiring two single residue insertions in the structure at $\alpha1$Thr-172 and $\alpha1$Gly-185 and the removal of the cytoplasmic loop between M3 and M4 ($\alpha1$Arg-313 to $\alpha1$Lys-383) and N- and C-terminal truncations. This model was placed within a membrane force field and partially minimized to eliminate high energy interactions induced by the $\alpha1$ sequence replacements (two cycles of minimization, final system energy = −211,878 kcal/mol). Although propofol, AziP*m*, or *o*-PD docked readily at the intersubunit anesthetic-binding site at the α^+-β^- interface, we were unable to dock to the β^+-α^- or β^+-β^- interfaces without modifying the side chain orientations of β3Asn-265 (βM2–15′) and/or α1Met-236 (in αM1). After these side chains were rotated out of the pockets, propofol was placed into the $\beta3$-$\alpha1$ or $\beta3$-$\beta3$ pocket, and the system was minimized for two cycles, followed by 10 additional cycles of minimization after removal of propofol. The CHARMm-based molecular dynamics simulated-annealing program CDOCKER was used to dock propofol, AziP*m*, and *o*-PD within the pockets in the transmembrane domain at the β^+-α^-, α^+-β^-, and β^+-β^- subunit interfaces and in the intersubunit pockets accessible from the ion channel in proximity to β3His-267 ($\beta3$ $GABA_AR$-based model only; no pocket in the GLIC-based model). We also docked the anesthetics at the top and bottom of the ion channel and in the intrasubunit pockets. Although no intrasubunit pockets were present in the $\beta3$ $GABA_AR$-based model, in the GLIC-based model β3His-267 contributed to the $\beta3$ subunit pocket. For the intersubunit sites, randomly oriented and randomly distributed molecules of propofol (9–30), AziP*m* (6–30), and *o*-PD (6) were seeded within binding site spheres (12 Å radii) centered on the proposed anesthetic-binding sites defined between M2–15′, the conserved proline in M1 (α1Pro-233/β3Pro-228), and the conserved aromatic residue in M3 (α1Tyr-294/β3Phe-289). For each binding site, CDOCKER was set up to first generate 10–40 random conformations for each replica using high temperature molecular dynamics, and 10–40 random orientations of each molecule were generated within the binding site spheres. The lowest 25–100 energy-minimized docking solutions, generated using simulated annealing and full potential minimization, were collected and ranked according to CDOCKER interaction energies. In the $\beta3$ $GABA_AR$ model, all three anesthetics were predicted to bind stably at the following: 1) each intersubunit anesthetic-binding site; 2) at each β3His-267-associated pocket near the ion channel; and 3) at the bottom of the ion channel at the levels of M2–2′-M2–6′. Less favorable binding was predicted in the ion channel at the level of M2–13′. Communication between the β-β intersubunit anesthetic sites and the β3His-267-associated pocket at the β-β interface near the ion channel was blocked by β3Pro-228 from M1 on the β^- side and from β3Thr-262 (M2–12′) and $\beta3$-Thr-266 (M2–16′) from M2 on the β^+ side in the crystal structure. In the GLIC-based model using CDOCKER interaction energies, AziP*m* and propofol were each predicted to bind with highest affinity at the β^+-α^- and β^+-β^- interface, and with lower affinity at the α^+-β^- interface and in the ion channel. No stable binding was predicted in the intrasubunit pockets.

Connolly surface representations defined by a 1.4-Å diameter probe of the ensemble of the 25 lowest CDOCKER interaction energy docking solutions for both propofol and AziP*m* are shown, along with the AziP*m* molecule docked with the lowest CDOCKER interaction energy, for the β^+-α^-, α^+-β^-, and

TABLE 1

Pharmacological specificity of *R*-[^{3}H]*m*TFD-MPAB photoincorporation into residues in the $\alpha1\beta3$ GABA$_A$R (cpm/pmol PTH-derivative)

Photolabeled amino acids were identified in $\alpha1\beta3$ GABA$_A$R purified in 0.2 mM asolectin, 5 mM CHAPS after photolabeling with 1.6 μM *R*-[^{3}H]*m*TFD-MPAB. The efficiency of photolabeling of a residue (in cpm/pmol) was calculated using Equation 3 (see "Experimental Procedures"). ND means not determined.

Amino acid	Control	+*R-m*TFD-MPAB (60 μM)	+Etomidate (200 μM)
βM1 β3Met-227	7,100	140	5,200
βM3 β3Met-286	170	14	8
βM3 β3Phe-289	220	10	8
αM3 α1Tyr-294	150	ND	ND

β^+-β^- intersubunit sites. Also shown in Connolly surface representation is the β-β intersubunit pocket accessible from the ion channel in proximity to β3His-267.

RESULTS

Propofol, AziPm, and o-PD Inhibit [^{3}H]Azietomidate and R-[^{3}H]mTFD-MPAB Photolabeling of $\alpha1\beta3$ GABA$_A$R—In $\alpha1\beta3$, as in $\alpha1\beta3\gamma2$ GABA$_A$Rs, [^{3}H]azietomidate photolabels amino acids at the β^+-α^- subunit interface in βM3 (β3Met-286) and αM1 (α1Met-236) (16, 19), but the amino acids photolabeled at the α^+/γ^+-β^- interfaces by *R*-[^{3}H]*m*TFD-MPAB had been identified only in the $\alpha1\beta3\gamma2$ GABA$_A$R (19). Here, we found that in the $\alpha1\beta3$ GABA$_A$R also *R*-[^{3}H]*m*TFD-MPAB photolabeled β3Met-227 in βM1 most efficiently, with β3Met-286 and β3Phe-289 photolabeled at ~3% that level (Table 1). Like in the $\alpha1\beta3\gamma2$ GABA$_A$R, *R-m*TFD-MPAB (60 μM) inhibited photolabeling of β3Met-227 by >98%, although etomidate (200 μM) inhibited by <25%. Both *R-m*TFD-MPAB and etomidate inhibited β3Met-286 and β3Phe-289 photolabeling by >90%.

The concentration dependence of inhibition of [^{3}H]azietomidate or *R*-[^{3}H]*m*TFD-MPAB $\alpha1\beta3$ GABA$_A$R photolabeling by anesthetic drugs was determined at the level of subunits resolved by SDS-PAGE (Fig. 2 and Table 2). Etomidate was a potent inhibitor of [^{3}H]azietomidate photolabeling (IC_{50} = 1.6 ± 0.3 μM), although at 300 μM it inhibited *R*-[^{3}H]*m*TFD-MPAB photolabeling by only 30%. *R-m*TFD-MPAB was ~50-fold more potent as an inhibitor of *R*-[^{3}H]*m*TFD-MPAB (IC_{50} = 1.4 ± 0.4 μM) than of [^{3}H]azietomidate (IC_{50} = 69 ± 14 μM) photolabeling. Propofol, AziP*m*, and *o*-PD each produced concentration-dependent inhibition of [^{3}H]azietomidate or *R*-[^{3}H]*m*TFD-MPAB photolabeling consistent with competitive inhibition. [^{3}H]Azietomidate photolabeling was inhibited by propofol, AziP*m*, and *o*-PD with IC_{50} values of 13 ± 2, 10 ± 3, and 13 ± 2 μM, respectively. AziP*m* (IC_{50} = 8 ± 4 μM) was ~6-fold more potent than propofol (IC_{50} = 44 ± 8 μM) or *o*-PD (IC_{50} = 54 ± 4 μM) as an inhibitor of *R*-[^{3}H]*m*TFD-MPAB photolabeling.

[^{3}H]AziPm Photoincorporation in $\alpha1\beta3$ GABA$_A$R Is Inhibitable by Propofol, Etomidate, and R-mTFD-MPAB—When $\alpha1\beta3$ GABA$_A$Rs were photolabeled on an analytical scale with [^{3}H]AziP*m*, 300 μM propofol inhibited photolabeling in α1 and β3 subunits by ~30 and 50%, respectively, and 100 μM etomidate or *R-m*TFD-MPAB, alone or in combination, inhibited β subunit photolabeling by 60% (Fig. 3). We also found that nonradioactive AziP*m* at 30 μM inhibited subunit photolabeling to the same extent as propofol (data not shown). Although at the level of intact GABA$_A$R subunits ~90% of [^{3}H]azietomidate and *R*-[^{3}H]*m*TFD-MPAB photolabeling was pharmacologically specific (Fig. 2), for [^{3}H]AziP*m*, ≤60% of subunit photolabeling was inhibitable by high concentrations of anesthetics. The residual ^{3}H incorporation probably reflects "nonspecific" photolabeling at the GABA$_A$R-detergent/lipid interface, as has been seen in studies of nAChR photolabeling by [^{3}H]AziP*m* (22) and other photoreactive general anesthetics (33, 34) and hydrophobic probes (35). Based upon the amount of GABA$_A$R photolabeled (3.5 pmol of [^{3}H]muscimol sites) and the radiochemical specific activity of [^{3}H]AziP*m* (10 Ci/mmol), the 5,500 cpm of propofol-inhibitable incorporation in the β3 subunit gel bands (~1,000 cpm/pmol β3 subunit) indicated photolabeling of ~10% of β3 subunits, and the ~1,000 ^{3}H cpm of propofol-inhibitable α1 subunit incorporation (280 cpm/pmol) indicated photolabeling of 3% of α1 subunits. We also determined the concentration dependence of the inhibition of [^{3}H]AziP*m* photolabeling by these anesthetics (Fig. 3*C* and Table 2). *R-m*TFD-MPAB and etomidate inhibited [^{3}H]AziP*m* photoincorporation in the β3 subunit with IC_{50} values of 0.8 ± 0.1 and 0.7 ± 0.2 μM, *i.e.* with concentration dependences consistent with *R-m*TFD-MPAB binding to its site at the α^+-β^- interface and etomidate binding at the β^+-α^- interface. Propofol inhibited [^{3}H]AziP*m* photolabeling with an IC_{50} of 7 ± 3 μM.

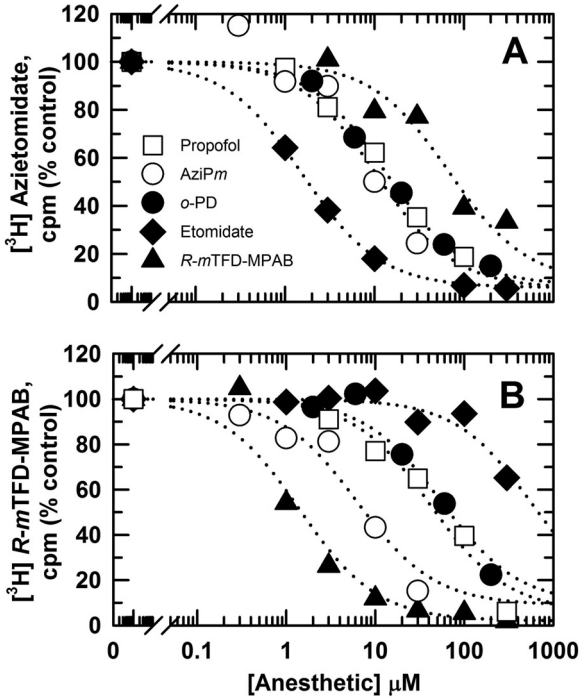

FIGURE 2. **Inhibition of [^{3}H]azietomidate (*A*) and *R*-[^{3}H]*m*TFD-MPAB (*B*) photolabeling by propofol, AziP*m*, and *o*-PD.** $\alpha1\beta3$ GABA$_A$Rs purified in 0.2 mM asolectin, 5 mM CHAPS (3.5 pmol of [^{3}H]muscimol-binding sites) were photolabeled in the presence of 0.9 μM [^{3}H]azietomidate or 1 μM *R*-[^{3}H]*m*TFD-MPAB in the presence of propofol (□), AziP*m* (○), *o*-PD (●), etomidate (♦), and nonradioactive *R-m*TFD-MPAB (▲). For each condition, plotted values are the average inhibition from two independent photolabeling experiments. The concentration dependences of inhibition were fit independently for each experiment as described under "Experimental Procedures," and the means of the IC_{50} values (± range), the total anesthetic concentration reducing specific photolabeling by 50%, are tabulated in Table 2.

TABLE 2

Anesthetic affinities for $\alpha1\beta3$ GABA$_A$R anesthetic-binding sites

IC_{50} values, the total anesthetic concentrations resulting in 50% inhibition of photolabeling of $\alpha1\beta3$ GABA$_A$R purified in 0.2 mM asolectin, 5 mM CHAPS, were determined as described under "Experimental Procedures" (mean ± range, two independent experiments); EC_{50} value for anesthesia, tadpole loss of righting reflex.

Drug	*R*-[^{3}H]Azietomidate IC_{50}	*R*-[^{3}H]*m*TFD-MPAB IC_{50}	[^{3}H]AziP*m* IC_{50}	EC_{50} anesthesia	Partition coefficient
	μM	μM	μM	μM	
R-Etomidate	1.6 ± 0.3 2.5 ± 0.3[a]	580 ± 110	0.5 ± 0.2 2.1 ± 0.5[a]	2.3[b]	300[b]
R-*m*TFD-MPAB	69 ± 14	1.4 ± 0.4	0.7 ± 0.3	3.7[c]	6,200[c]
Propofol	13 ± 2 46 ± 3[a]	44 ± 8	8 ± 2 25 ± 4[a]	3[d] 4.7[f] (mg/kg)	6,200[e]
AziP*m*	10 ± 3 21 ± 4[a]	8 ± 4	7 ± 2[a]	3[d]	8,500[e]
o-PD	13 ± 2	54 ± 4	ND[f]	14.7[f] (mg/kg)	4,900[e]

[a] IC_{50} values for $\alpha1\beta3$ GABA$_A$R purified in 0.86 mM asolectin, 11.5 mM cholate are shown.
[b] From Ref. 26.
[c] From Ref. 25.
[d] From Ref. 21.
[e] XLOGP3 (46) was calculated with the ALOPS2.1 Program, VCCLAB, Virtual Computational Chemistry.
[f] Rat loss of righting reflex is shown in mg/kg (21); ND means not determined.

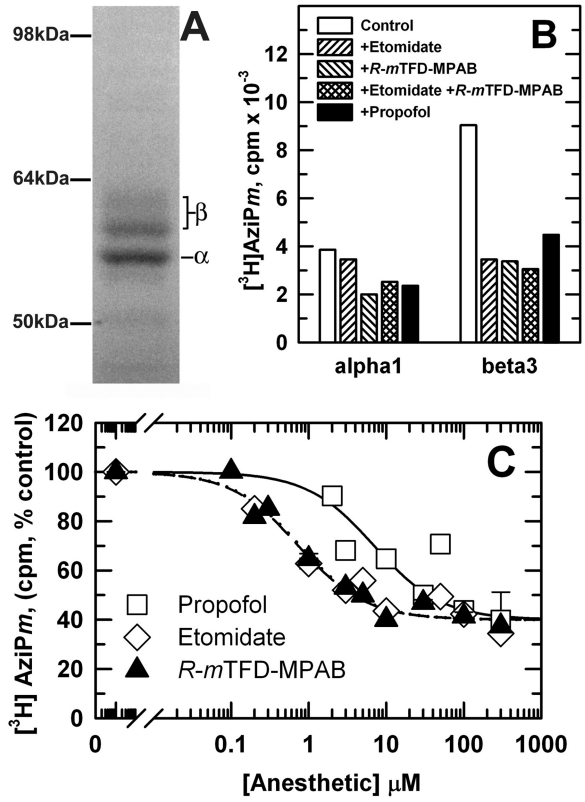

FIGURE 3. **[^{3}H]AziP*m* photolabeling of $\alpha1\beta3$ GABA$_A$R is inhibitable by propofol, etomidate, and *R*-*m*TFD-MPAB.** $\alpha1\beta3$ GABA$_A$R, equilibrated with 1 mM GABA, was photolabeled with [^{3}H]AziP*m* in the absence or presence of propofol, etomidate, or *R*-*m*TFD-MPAB, and aliquots (~ 3.5 pmol [^{3}H]muscimol-binding sites) were fractionated by SDS-PAGE. *A*, Coomassie Blue stain of a representative gel lane. The subunit compositions of the three stained gel bands were characterized previously by N-terminal sequence analysis (16); the ~56-kDa band contained primarily the α1 subunit, and the ~59 and ~61-kDa bands contained differentially glycosylated β3 subunits. Subunit cross-contamination was ~10%. *B* and *C*, ^{3}H incorporation into GABA$_A$R subunits, determined by liquid scintillation counting of the subunit bands excised from the gel. *B*, [^{3}H]AziP*m* (8 μM) subunit photolabeling in the absence or presence of 100 μM etomidate, 100 μM *R*-*m*TFD-MPAB, singly or combined, or 300 μM propofol. *C*, concentration dependence of inhibition of [^{3}H]AziP*m* (4 μM) β subunit photolabeling by propofol (□), etomidate (◇), or *R*-*m*TFD-MPAB (▲). For each drug, data were combined from two experiments using the same purification of GABA$_A$R. The means of IC_{50} values (± range) calculated independently from each experiment are tabulated in Table 2.

Localization of GABA$_A$R Structural Domains Containing Amino Acids Photolabeled by [^{3}H]AziPm—To provide an initial characterization of the GABA$_A$R subunit regions containing photolabeled amino acids, GABA$_A$Rs were photolabeled on a preparative scale with [^{3}H]AziP*m* in the absence and presence of propofol, and rpHPLC was used to fractionate EndoLys-C and EndoGlu-C digests of material eluted from the gel bands enriched in β3 subunits (Fig. 4) and α1 subunits (data not shown). For both digests, all ^{3}H was eluted in two broad peaks in a region of the gradient (50–70% solvent B) reported previously to contain fragments beginning near the N terminus of the M1 and M3 helices (16), and no ^{3}H was recovered in the hydrophilic fractions containing fragments from extracellular domains of GABA$_A$R subunits.

Aliquots of the EndoLys-C digests of labeled α1 and β3 subunits were sequenced to identify the cycles of Edman degradation with peaks of ^{3}H release indicative of the presence of a photolabeled amino acid (Fig. 5). In the α1 subunit digest, there were peaks of ^{3}H release in cycles 17 and 19. In the β3 subunit digest, there was a peak of ^{3}H release in cycle 12. Because the digests contained all subunit fragments, peaks of ^{3}H release could not be directly associated with specific subunit fragments. However, based upon the rpHPLC fractionation of the subunit digests, [^{3}H]AziP*m* was likely to be incorporated into one or more of the subunit transmembrane helices. For each subunit, digestion with EndoLys-C produced fragments beginning before the M1, M3, and M4 helices (Fig. 5). Therefore, for the α1 subunit digest, the peaks of ^{3}H release in cycles 17 and 19 would be consistent with photolabeling in αM1 of α1Ile-239 in the fragments beginning at α1Arg-223 or α1Ile-221, respectively. For the β3 subunit digest, the peak of ^{3}H release in cycle 12 was consistent with photolabeling in β3M1 of β3Met-227, the amino acid photolabeled by *R*-[^{3}H]*m*TFD-MPAB (Table 2) (19).

[^{3}H]AziPm Photolabels α1Ile-239 and α1Met-236 in αM1—To identify photolabeled amino acids, $\alpha1\beta3$ GABA$_A$Rs were photolabeled with [^{3}H]AziP*m* on a preparative scale (~60 pmol of [^{3}H]muscimol-binding sites per condition) in the absence or presence of propofol, and samples enriched in α1 or β3 subunits were isolated by SDS-PAGE. Two complementary sequencing strategies established that there was propofol-inhibitable photolabeling of α1Ile-239 by [^{3}H]AziP*m* (Fig. 6). First, an EndoLys-C digest of the α1 subunit was sequenced with OPA treatment in cycle 11 (at α1Pro-233) to prevent further sequencing of other fragments not containing a proline at

that cycle (18, 31). After OPA treatment, the fragment beginning at α1Ile-223 was the primary sequence, and the peak of ^{3}H release at cycle 17 was consistent with photolabeling of α1Ile-239, with propofol inhibiting photolabeling by ~60% (Fig. 6*A*). The minor peak of ^{3}H release at cycle 14 was consistent with propofol-inhibitable photolabeling of α1Met-236, the amino acid in αM1 photolabeled by [^{3}H]azietomidate and [^{3}H]TDBzl-

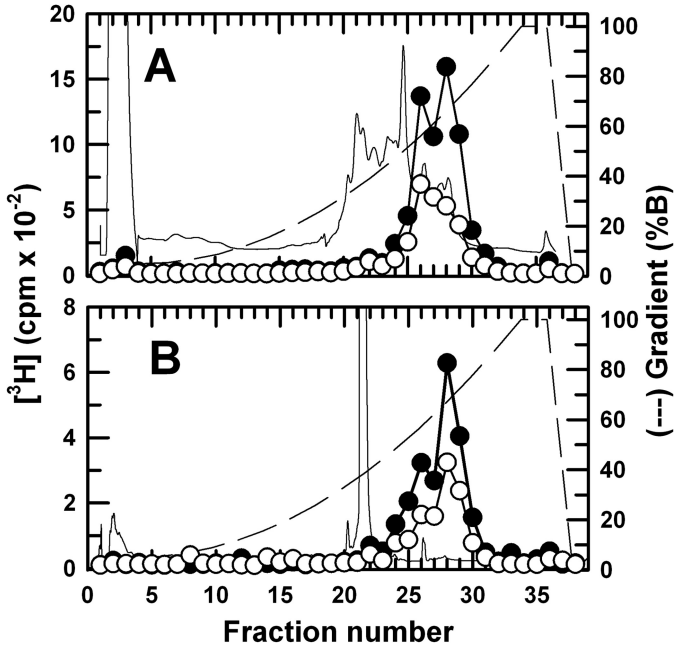

FIGURE 4. **Reverse-phase HPLC fractionation of EndoLys-C (*A*) and Endo-Glu-C (*B*) of digests of [^{3}H]AziP*m*-photolabeled GABA$_A$R β3 subunit.** The β3 subunits were isolated by SDS-PAGE from α1β3 GABA$_A$Rs photolabeled on a preparative scale (~60 pmol [^{3}H]muscimol-binding sites) with 8 μM [^{3}H]AziP*m* in the presence of GABA ± 300 μM propofol (PPF). The ^{3}H elution profiles (−PPF, ●; +PPF, ○) were determined by liquid scintillation counting of 10% of each fraction, and absorbance was monitored at 215 nm (−PPF, *continuous line*). The elution gradient (% solvent *B*) is indicated by the *dashed lines*.

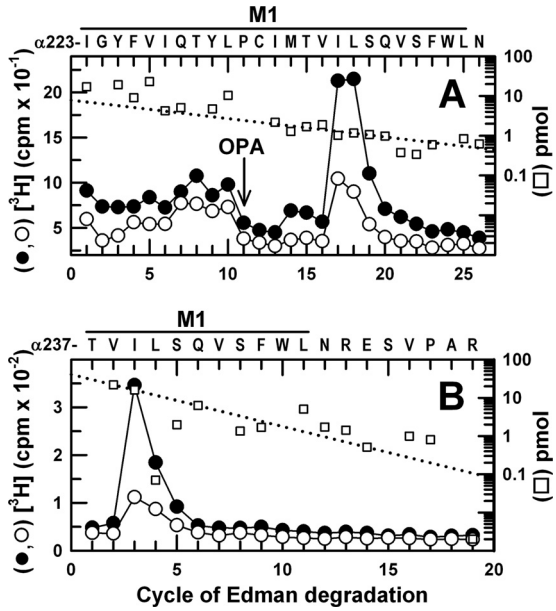

FIGURE 6. **[^{3}H]AziP*m* photolabels α1M1-Ile-239 in αM1.** ^{3}H (●, ○) and PTH-derivatives (□) released during sequencing of α1 subunit fragments beginning at α1Ile-223 (*A*) and α1Thr-237 (*B*). *A,* EndoLys-C digests of α1 subunits from α1β3 GABA$_A$Rs photolabeled by 11 μM [^{3}H]AziP*m* in the absence (●, □) or presence (○) of 100 μM propofol were loaded directly onto PVDF filters and sequenced, with OPA treatment in cycle 11 to chemically isolate during further sequencing the α1M1 fragment with α1Pro-233 in that cycle. After OPA treatment, the primary sequence began at α1Thr-223 (I_0 = 10 pmol, both conditions), with a secondary sequence beginning at αIle-392 (I_0 = 3 pmol). The peak of ^{3}H release in cycle 17 was consistent with photolabeling of α1Ile-239 in the primary sequence (−PPF/+PPF, 244/114 cpm/pmol), and the minor peak of ^{3}H release in cycle 14 indicated photolabeling of α1Met-236 (−PPF/+PPF, 27/7 cpm/pmol). *B,* EndoGlu-C digests of α1 subunits from GABA$_A$Rs photolabeled by 8 μM [^{3}H]AziP*m* in the absence (●, □) or presence (○) of 300 μM propofol were fractionated by rpHPLC, and fractions containing the peak of ^{3}H were loaded onto glass fiber filters, treated with CNBr (see "Experimental Procedures"), and sequenced. The primary sequence began at αThr-237 within α1M1 (□, I_0 = 40 pmol, both conditions), with secondary sequences beginning at αAsp-287 at the N terminus of αM3 (I_0 = 20 pmol) and a contaminating β3 subunit fragment beginning at β3Gly-287 in βM3 (I_0 = 10 pmol). The peak of ^{3}H release in cycle 3 was consistent with photolabeling of αIle-239.

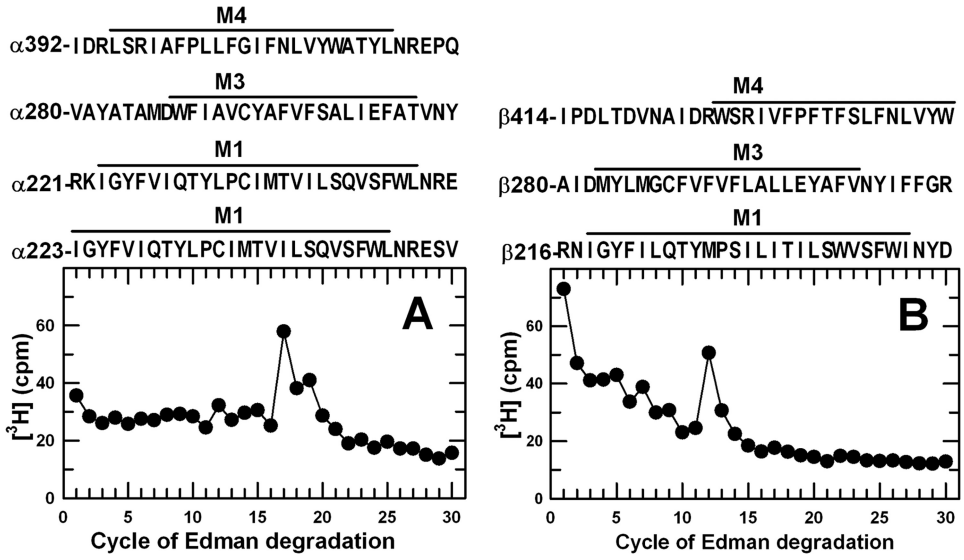

FIGURE 5. **^{3}H release profiles obtained by N-terminal sequence analysis of EndoLys-C digests of α1 and β3 subunits isolated from [^{3}H]AziP*m*-photolabeled GABA$_A$R.** Digests of α1 (*A*) and β3 ($\beta3_{59\ kDa}$, *B*) subunits isolated from GABA$_A$Rs photolabeled with 11 μM [^{3}H]AziP*m* were loaded directly onto PVDF sequencing filters without prior purification by rpHPLC. Included *above* each panel are the subunit fragment sequences containing transmembrane helices that can be produced by EndoLys-C digestion. In this experiment, 3,850 cpm of α subunit and 5,125 cpm of β subunit digests (−PPF) were loaded on filters, and 4/5 of the material from each cycle of Edman degradation was collected for determination of released ^{3}H.

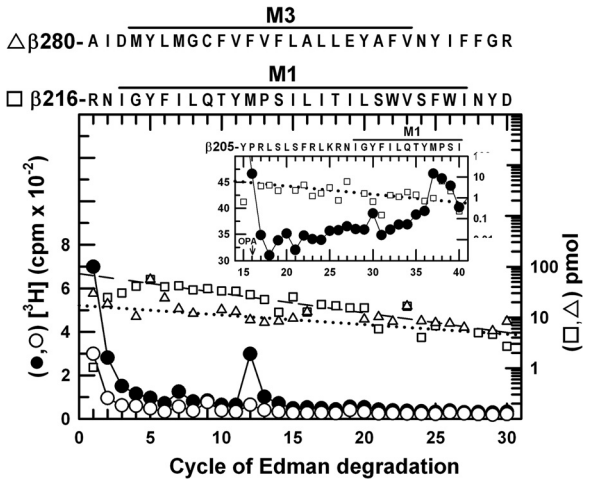

FIGURE 7. **[^{3}H]AziP*m* photolabels β3Met-227 in βM1.** ^{3}H (●, ○) and PTH-derivatives (□, △) released during sequencing of fragments isolated by rpHPLC (Fig. 4*A*, fractions 27–29) from EndoLys-C digests of β3. The primary sequence began at β3Arg-216 near the N terminus of βM1 (□, I_0 = 70 pmol, both conditions), with a secondary sequence beginning at β3Ala-280 before βM3 (△, I_0 = 18 pmol, both conditions). The peak of ^{3}H release in cycle 12 indicated photolabeling of β3Met-227 in βM1 (−PPF/+PPF, 18/3 cpm/pmol). *Inset*, direct sequencing of an EndoGlu-C digest of photolabeled $\beta3_{59\ kDa}$, with OPA treatment in cycle 16 to chemically isolate during further sequencing the fragment beginning at β3His-191 (25 pmol) that contains β3Pro-206 in cycle 16 and extends through βM1. The peak of ^{3}H release in cycle 37 confirmed photolabeling of β3Met-227 (18 cpm/pmol, −PPF).

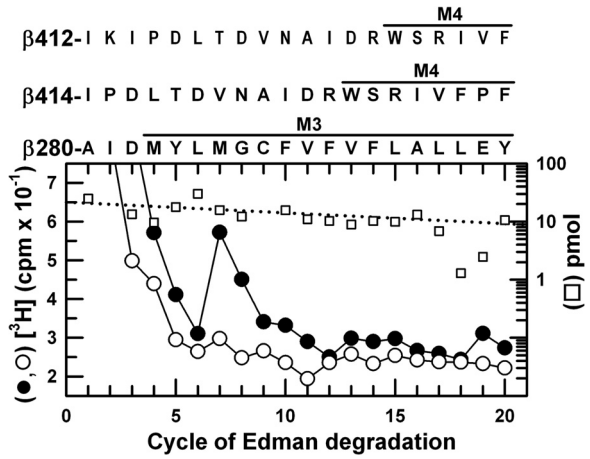

FIGURE 8. **[^{3}H]AziP*m* photolabels β3M3-Met-286 in βM3.** ^{3}H (●, ○) and PTH-derivatives (□) released during sequencing of fragments isolated by rpHPLC (Fig. 4*A*, fractions 25–26) from EndoLys-C digests of β3 subunits. The major fragments present began at β3Ala-280 before βM3 (□, I_0 = 21 pmol, both conditions) and fragments beginning before βM4 at β3Ile-412 (20 pmol, both conditions) and β3Ile-414 (26 pmol, both conditions). The peak of ^{3}H release in cycle 7 indicated photolabeling of β3Met-286 in βM3 (−PPF/+PPF: 3/0.4 cpm/pmol). The minor peak of ^{3}H release in cycle 7 when HPLC fractions 27–29 were sequenced (Fig. 7) was also consistent with propofol-inhibitable photolabeling of β3Met-286.

etomidate (16). As the fragment beginning before αM4 at α1Ile-392 was present as a secondary sequence after OPA treatment in cycle 11 (due to the presence α1Pro-401), we used an alternative sequencing strategy to confirm photolabeling of α1Ile-239 that depended upon CNBr cleavage at α1Met-236. When the fragment beginning at α1Thr-237 was sequenced for 25 cycles, there was a peak of ^{3}H release only in cycle 3, consistent with photolabeling of α1Ile-239 (Fig. 6*B*).

[^{3}H]AziPm Photolabels β3Met-227 in βM1 and β3Met-286 in βM3—EndoLys-C digests of photolabeled β subunits were fractionated by rpHPLC, and the two peaks of ^{3}H (Fig. 4*A*) were pooled separately for sequence analysis (Figs. 7 and 8). The more hydrophobic peak (Fig. 7) contained as the primary sequence the fragment beginning at β3Arg-216 near the N terminus of βM1 (70 pmol) and a secondary sequence beginning at β3Ala-280, the N terminus of βM3 (18 pmol). The major peak of ^{3}H release in cycle 12 would correspond to photolabeling in the primary sequence of β3Met-227 within βM1, with propofol inhibiting photolabeling by ~85%. Photolabeling of β3Met-227 was confirmed by the peak of ^{3}H release seen in cycle 37 when a fragment beginning at β3His-191 was sequenced with OPA treatment in cycle 16 (β3Pro-206) (Fig. 7, *inset*). The peak of ^{3}H eluting first in the rpHPLC fractionation contained the fragment beginning at β3Ala-280 (20 pmol) and fragments beginning before βM4 at β3–414 (26 pmol) and β3–412 (19 pmol) (Fig. 8). The peak of ^{3}H release in cycle 7 indicated propofol-inhibitable photolabeling of β3Met-286 within βM3, because that release could not result from photolabeling of β3Val-420 before βM4 in the absence of a peak of ^{3}H release in cycle 9 from that position in the β3Ile-412 fragment.[3]

[^{3}H]AziPm Photolabeling in Other Transmembrane Helices—Photolabeling within βM2, if it occurred, was at <15% the efficiency of β3Met-227, based upon the levels of ^{3}H released during sequencing of a sample containing the fragment beginning at β3Ile-242 (11 pmol), produced by BNPS-skatole cleavage at β3Trp-241. Photolabeling within αM2, if it occurred, was at <10% the efficiency of α1Ile-239, based upon sequence analysis of the fragment beginning before αM2 at α1Ser-251 (6 pmol) produced by subunit digestion with EndoGlu-C and then chemical isolation of that fragment during sequence analysis by treatment with OPA at cycle 3. Photoincorporation within αM3 was characterized when the fragment beginning at α1Asp-287 was sequenced along with the fragment beginning at α1Thr-237 (Fig. 6*B*). Because no peak of ^{3}H release was detected other than the peak in cycle 3 expected for the photolabeling of α1Ile-239, any photolabeling in αM3 was at <15% the efficiency of α1Ile-239.

DISCUSSION

In this study, we characterize the interactions of propofol with the α1β3 GABA$_A$R by directly identifying the GABA$_A$R amino acids photolabeled by [^{3}H]AziP*m*, a photoreactive propofol analog, and by comparing propofol, AziP*m*, and *o*-PD interactions with the intersubunit anesthetic-binding sites identified by [^{3}H]azietomidate and *R*-[^{3}H]*m*TFD-MPAB (16, 19). When photolabeling was analyzed at the level of GABA$_A$R subunits, we found that propofol, AziP*m*, and *o*-PD each inhibited [^{3}H]azietomidate or *R*-[^{3}H]*m*TFD-MPAB photolabeling in a manner consistent with competitive inhibition, and con-

[3] Sequence analyses of β3 subunit fragments isolated by rpHPLC were characterized by substantial, decreasing "wash-off" of ^{3}H in the first 3–4 cycles of Edman degradation for samples enriched in βM1-βM2 (Fig. 7) or βM3/βM4 (Fig. 8) that was not seen for α1 subunit samples. The source is unknown for this incorporation that is unstable under the acid and/or base treatments necessary for Edman degradation, but there was no evidence of unstable ^{3}H incorporation when enzymatic digests of β subunits were fractionated by rpHPLC in 0.1% trifluoroacetic acid (Fig. 4).

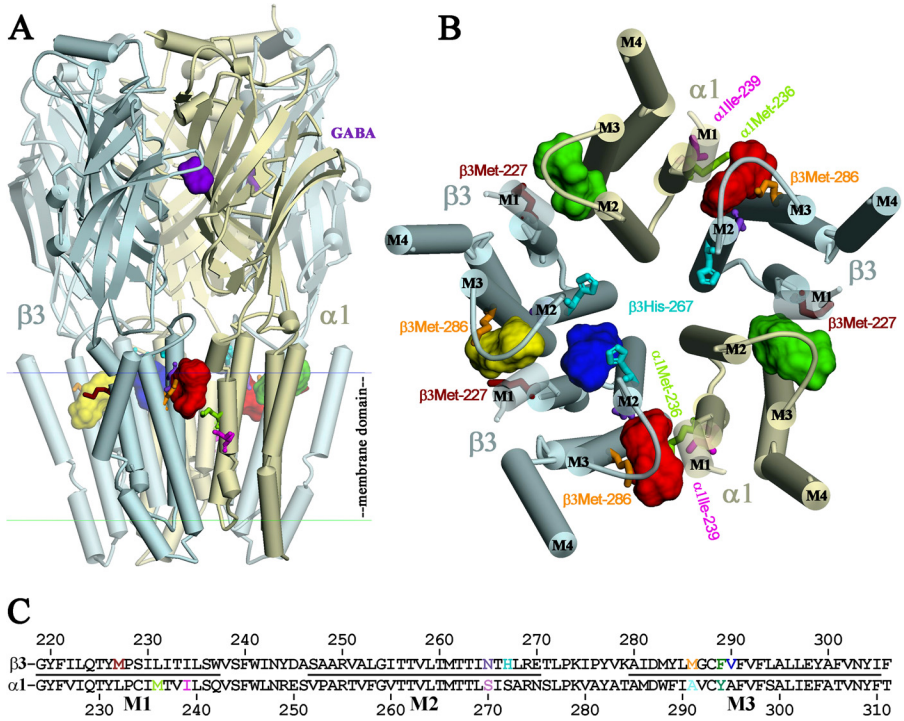

FIGURE 9. **AziP*m*-binding sites in the α1β3 GABA$_A$R TMD at the β^+-α^-, α^+-β^-, and β^+-β^- subunit interfaces.** Views of an α1β3 GABA$_A$R homology model built using a β3 GABA$_A$R crystal structure (Protein Data Bank code 4COF) from the side (*A*) and of the TMD from the base of the extracellular domain (*B*), with α-helices displayed as *cylinders*, β-sheets as *ribbons*, and subunits color-coded as follows: α1, *yellow*; β3, *blue*. The agonist benzamidine (*purple*) from the 4COF structure is shown in the extracellular domain at the β^+-α^- subunit interface. The locations in the TMD of the homologous intersubunit general anesthetic-binding sites identified by photoaffinity labeling with [^{3}H]azietomidate, *R*-[^{3}H]*m*TFD-MPAB, or [^{3}H]AziP*m* are indicated at the β^+-α^- (*red*), α^+-β^- (*green*), and β^+-β^- (*yellow*) subunit interfaces as the Connolly surface representations of 25 AziPm and 25 propofol docked in their most energetically favorable orientations. Also shown at the β^+-β^- subunit interface is a potential propofol binding pocket accessible from the ion channel (*blue*). *C*, aligned GABA$_A$R α1 and β3 subunit sequences spanning the M1–M3 helices with residues that are photolabeled color-coded as in *A* and *B* and in Fig. 10.

versely, propofol, etomidate, and *R*-*m*TFD-MPAB each inhibited [^{3}H]AziP*m* photoincorporation to a similar extent.[4] It was surprising that etomidate or *R*-*m*TFD-MPAB each inhibited [^{3}H]AziP*m* β subunit photolabeling to the same extent and with IC_{50} values of 1 μM because they bind with high affinity and selectivity at the β^+-α^- and α^+-β^- subunit interfaces, respectively, and they do not inhibit each other's photolabeling at those sites with high affinity. However, in the α1β3 GABA$_A$R, etomidate and *R*-*m*TFD-MPAB were both potent inhibitors of *R*-[^{3}H]*m*TFD-MPAB photolabeling of β3Met-286 and β3Phe-289, but only *R*-*m*TFD-MPAB was a potent inhibitor of photolabeling of β3Met-227, the amino acid accounting for ~95% of ^{3}H incorporation in the β subunit (Table 1). This indicates that in the α1β3 GABA$_A$R, both *R*-*m*TFD-MPAB and etomidate (16) bind with high affinity to the homologous site at the β^+-β^- subunit interface and that [^{3}H]AziP*m* may be preferentially photolabeling amino acids at that interface.

Protein microsequencing identified propofol-inhibitable photolabeling by [^{3}H]AziP*m* of amino acids in the etomidate site at the GABA$_A$R β^+-α^- subunit interface (α1Met-236/α1Ile-239 in αM1 and β3Met-286 in βM3) and in the *R*-*m*TFD-MPAB site at the α^+-β^- subunit interface (β3Met-227 in βM1). β3Met-286 and β3Met-227 are also present at the β^+-β^- interface of an α1β3 GABA$_A$R that does not occur in an α1β3γ2 GABA$_A$R. However, AziP*m* clearly binds in proximity to β3Met-227 in βM1 at the α^+-β^- interface because AziP*m* inhibits *R*-[^{3}H]*m*TFD-MPAB β subunit photolabeling but etomidate does not. As discussed above, the concentration dependence of *R*-*m*TFD-MPAB and etomidate inhibition of [^{3}H]AziP*m* β subunit photolabeling indicates that [^{3}H]AziP*m* also photolabels amino acids at the β^+-β^- intersubunit site.

The IC_{50} values for inhibition of photolabeling in the α subunit by [^{3}H]azietomidate and in the β subunit by *R*-[^{3}H]*m*TFD-MPAB define the apparent affinities of anesthetics for the sites at the two β^+-α^- and two α^+-β^- interface sites per α1β3 GABA$_A$R, respectively. Inhibition of [^{3}H]AziP*m* photolabeling in the β subunit defines anesthetic affinity for the site at the β^+-β^- interface (Table 2). [^{3}H]AziP*m* did not identify novel anesthetic-binding sites but did bind with high affinity (IC_{50} values ~5–10 μM) to each of the classes of intersubunit sites. Propofol and *o*-PD bind with ~3-fold higher affinity to the β^+-α^- ([^{3}H]azietomidate, IC_{50} = 13 μM) sites than to the α^+-β^- (*R*-[^{3}H]*m*TFD-MPAB, IC_{50} ~ 50 μM) sites, and propofol also binds with high affinity at the β^+-β^- site ([^{3}H]AziP*m*, IC_{50} = 8 μM). Taken together, our results provide further evidence that propofol modulation of GABA$_A$R function results from propofol binding to the intersubunit sites.

The locations of these three classes of homologous intersubunit anesthetic-binding sites in the GABA$_A$R transmembrane domain are shown in Fig. 9 in a homology model of a β3β3α1β3α1 GABA$_A$R based upon the structure of the homomeric β3 GABA$_A$R (11), along with the location at the β^+-β^-

[4] *o*-PD inhibition of [^{3}H]AziP*m* photolabeling was not tested because supplies of [^{3}H]AziP*m* were exhausted before *o*-PD was synthesized.

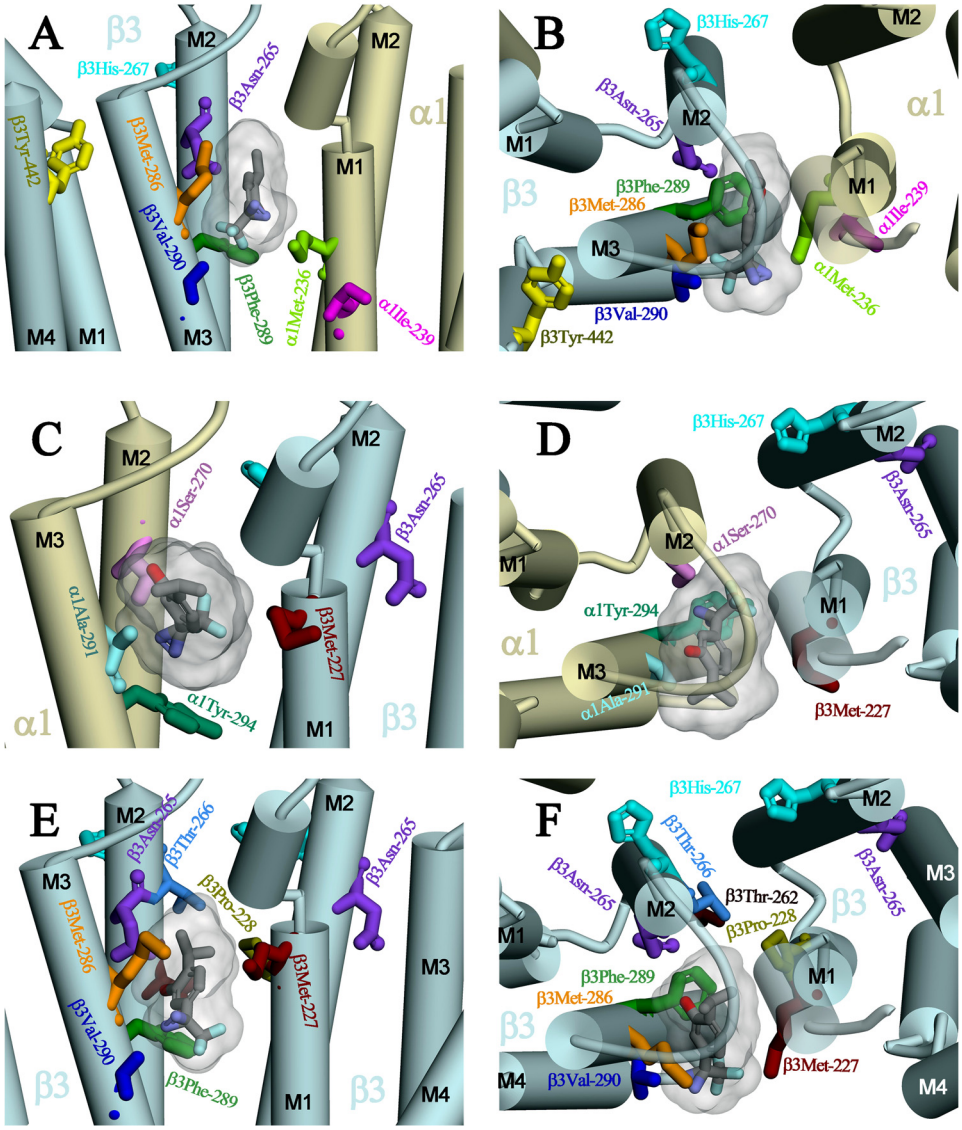

FIGURE 10. **Expanded views from the lipid (*A, C,* and *E*) or from the base of the extracellular domain (*B, D,* and *F*) of the general anesthetic-binding sites at the β^+-α^- (*A* and *B*), α^+-β^- (*C* and *D*), and β^+-β^- (*E* and *F*) subunit interfaces.** Shown in *stick* format are the residues photolabeled at the β^+-α^- interface by [^{3}H]AziP*m* (α1Ile-239 in *red*), by [^{3}H]AziP*m*, [^{3}H]azietomidate, and [^{3}H]TDBzl-etomidate (β3Met-286 in *orange* and α1Met-236 in *light green*), or by [^{3}H]TDBzl-etomidate (β3Val-290, *blue*) (16) or at the α^+-β^- interface by [^{3}H]AziP*m* and *R*-[^{3}H]*m*TFD-MPAB (β3Met-227 in *magenta*) or by *R*-[^{3}H]*m*TFD-MPAB (α1Ala-291 in *cyan* and α1Tyr-294, *dark green* (19)). Also highlighted are βHis-267, photolabeled by *o*-PD (20), and the propofol sensitivity determinants identified by mutational analyses (β3Asn-265 (βM2–15′) (3, 7) and β3Tyr-442 (9)). Shown in each binding site in Connolly surface representation are the volumes of the 25 lowest CDOCKER interaction energy solutions for both AziP*m* and propofol and an AziP*m* molecule docked in its lowest energy orientation, color-coded by atom type (carbon in *gray*; oxygen in *red*; nitrogen in *blue*; and fluorine in *cyan*). AziP*m* and propofol each have volumes of 182 Å^3, with the 50 lowest energy poses contained within volumes of 316, 400, and 318 Å^3 at the β^+-α^-, α^+-β^-, β^+-β^- interfaces, respectively.

interface of a pocket accessible from the ion channel and in contact with β3His-267, the residue photolabeled by *o*-PD (20). Also included in the figure is an alignment of α1 and β3 subunit sequences in the M1–M3 transmembrane domain with the photolabeled amino acids highlighted.

Expanded views of the intersubunit-binding sites are shown in Fig. 10 with AziP*m* docked in the lowest energy orientation predicted by computational docking and the amino acids identified in αM1, βM1, and βM3 that are photolabeled by [^{3}H]AziP*m* and in βM2 by *o*-PD (β3His-267 (βM2–17′) (20)). Also highlighted are the amino acids photolabeled by photoreactive etomidates and *R*-*m*TFD-MPAB and those identified by mutational analyses as propofol sensitivity determinants (β3M2–15′ (β3Asn-265), β3M3–4′ (β3Met-286), and β3Tyr-442 in βM4 (7–9)). β3Asn-265, the *in vitro* (7) and *in vivo* (3) sensitivity determinant, as well as the photolabeled/sensitivity determinant β3Met-286 and photolabeled α1Met-236 all contribute to the pocket at the β^+-α^- interface between the βM2/βM3 and αM2/αM1 helices (Fig. 10, *A* and *B*). Photolabeled αIle-239 is located at the same interface, approximately one helical turn below α1Met-236 and more lipid-exposed. Analyses of the reactivities of Cys mutant $GABA_ARs$ identify state-dependent changes in the structure of the β^+-α^- subunit interface at the level of α1Met-236 and β3Met-286 (36), although the studies do not determine whether those changes involve rotations of helices that would bring α1Ile-239 more into the subunit interface. β3Tyr-442 in βM4 is within 8 Å of β3Met-286 and β3Val-

290 in βM3, and this close proximity makes it likely that replacement of β3Tyr-442 by a bulkier Trp (9) will perturb the structure of the pocket at the β^+-α^- interface.

The photolabeled β3Met-227 in βM1, also photolabeled by *R*-[^{3}H]*m*TFD-MPAB, is located at the α^+-β^- interface between the αM2/αM3 and βM2/βM1 helices (Fig. 10, *C* and *D*) and at the β^+-β^- interface (Fig. 10, *E* and *F*). β3His-267, photolabeled by *o*-PD (20), contributes to the channel lumen and the interface between M2 helices, one helical turn above and ~11 Å from α1Ser-270 (αM2–15′) or β3Asn-265 (βM2–15′) and ~15 Å from β3Met-227. As noted in the structure of the β3 $GABA_AR$ (11), β3His-267 contributes to a potential propofol binding pocket that is accessible from the lumen of the ion channel. However, as shown in Fig. 10*F*, access to β3His-267 from the etomidate/*R*-*m*TFD-MPAB binding pocket at this interface is blocked by β3Thr-262 and β3Thr-266 (βM2–12′ and βM2–16′) from the β^+ subunit and β3Pro-228 from βM1 of the β^- subunit. Although our results establish that [^{3}H]AziP*m* photolabeling of βMet-227 and the amino acids in the other intersubunit-binding site was inhibited by propofol, it remains to be determined whether *o*-PD photolabeling of β3His-267 identifies a propofol-binding site because inhibition of photolabeling by propofol was not reported.

Docking and the Intersubunit Binding Sites—As in the $GABA_AR$ homology models based upon GLIC or GluCl (16, 19), in the model based upon the β3 $GABA_AR$, azietomidate (volume, 240 Å^3) and *R*-*m*TFD-MPAB (275 Å^3) are predicted to bind stably within each of the three classes of intersubunit pockets. Propofol and AziP*m*, which have the same molecular volumes (182 Å^3), as well as *o*-PD (volume, 150 Å^3), are also predicted to bind stably and with similar energies at each of the intersubunit pockets and also in the channel accessible pockets near β3His-267. It should be noted that the $GABA_AR$ we photolabeled was purified in the absence of cholesterol, although previous reconstitution studies indicate that cholesterol is essential for function (37, 38). Furthermore, it is probable that cholesterol actually binds the $GABA_AR$, and candidate sites would certainly include the intersubunit transmembrane cavities identified as anesthetic sites here (39, 40). However, bound cholesterol was not localized in the β3 $GABA_AR$ crystal structure, although the receptor was purified in the presence of 1 μM cholesterol (11), and the dimensions of the intersubunit pockets differ only subtly from those in GLIC or GluCl, purified in the absence of cholesterol (13, 15).

AziPm Photolabeling of Nonintersubunit-binding Sites—Although we did not identify photolabeled amino acids in regions other than the intersubunit-binding sites, the observed pharmacological specificity of [^{3}H]AziP*m* photolabeling at the level of the intact β subunit suggests that other photolabeled amino acids may remain to be identified. Although the efficiency of photolabeling of α1Ile-239 (240 cpm/pmol) was similar to the level of propofol-inhibitable α1 subunit photolabeling (~280 cpm/pmol), the levels of photolabeling of β3Met-227 (~20 cpm/pmol) or β3Met-286 (3 cpm/pmol) were much lower than the level of propofol-inhibitable β3 subunit photolabeling (~1,000 cpm/pmol, Fig. 3). Furthermore, the high levels of ^{3}H released in the first cycles of Edman degradation of samples enriched in fragments containing βM1-βM2 (Fig. 7) or βM3 (Fig. 8) suggest that ^{3}H is unstably incorporated into unidentified residues in those fragments and released during the acid or base treatments required for Edman degradation. For nAChR photolabeled by [^{3}H]AziP*m* (22), or in nAChR or $GABA_AR$ studies with [^{3}H]TDBzl-etomidate (16, 41) and *R*-[^{3}H]*m*TFD-MPAB (19, 34), which contain the same photoreactive trifluoromethylphenyl diazirine, no evidence was seen for similar apparent instability of photolabeled residues. Further studies using mass spectroscopic sequencing techniques may identify additional photolabeled amino acids in those fragments, which are likely to be located within the intersubunit-binding sites because *R*-*m*TFD-MPAB and etomidate are potent inhibitors of that photolabeling. This pharmacological specificity of the unidentified photolabeling in the β3 subunit makes it highly unlikely that it results from [^{3}H]AziP*m* photolabeling of β3His-267, the amino acid photolabeled by *o*-PD (20). Consistent with this, photolabeling of a nAChR histidine by [^{3}H]azioctanol, an aliphatic diazirine, was readily detected by Edman degradation (42).

Although AziP*m* and *o*-PD are both trifluoromethylphenyl diazirines, they may photoincorporate by different reactive intermediates. Their UV absorption spectra differ significantly. AziP*m* possesses a well resolved diazirine absorption band centered at 370 nm with an extinction coefficient (ϵ_{370} = 670 $M^{-1}cm^{-1}$) (21), similar to most trifluoromethylphenyl diazirines (43). *o*-PD has only a tailing absorption above 300 nm with $\epsilon_{350} = 70\ M^{-1}cm^{-1}$ (20). The fact that AziP*m* photolabels aliphatic and nucleophilic side chains is consistent with the reactivity expected for a carbene intermediate. Photoactivation of *o*-PD will lead to the formation of a 2-hydroxyphenylcarbene, which is predicted (44) to be 45 kcal/mol less stable than the o-quinone methide that can be formed by intramolecular rearrangement, a highly reactive electrophile that will react preferentially with nucleophilic amino acid side chains such as histidine (45).

AziPm as a Probe for Propofol-binding Sites in Pentameric Ligand-gated Ion Channels—Although the incorporation of a photoreactive diazirine in anesthetics as large as etomidate or MPAB can be accomplished with only minor perturbation of their core structures, the development of photoreactive analogs of anesthetics as small as propofol requires a more dramatic perturbation of structure. AziP*m* acts as a $GABA_AR$ modulator and tadpole anesthetic at similar concentrations as propofol (21). However, AziP*m* was of much lower efficacy than propofol as a modulator, and it inhibited GABA responses at concentrations above 3 μM, although propofol potentiated even at 30 μM (21). AziP*m* photolabeled amino acids in the propofol-binding sites identified by x-ray crystallography in apoferritin (21), a soluble model protein, and in GLIC, a proton-gated prokaryotic pentameric ligand-gated ion channel (23, 24).

Propofol and AziP*m* both inhibit the *Torpedo* nAChR. However, propofol binds preferentially to the nAChR in the desensitized state (+ agonist), and AziP*m* binds preferentially in the resting, closed channel state in the absence of agonist (22). [^{3}H]AziP*m* photolabeling identified three binding sites in the nAChR TMD as follows: (i) an intrasubunit site within the δ subunit helix bundle; (ii) a site in the ion channel, and (iii) a site at the γ-α interface (22). Photolabeling of the intrasubunit site,

which is equivalent to the propofol and AziP*m* site in GLIC, occurred in the desensitized state, but not the resting state, and propofol inhibited photolabeling competitively. Propofol also inhibited [^{3}H]AziP*m* photolabeling in the ion channel, but this inhibition was likely to be allosteric because photolabeling was also inhibited by agonist stabilization of the nAChR in the desensitized state. Propofol clearly did not bind to the site at the γ-α interface, because it potentiated rather than inhibited photolabeling. The photolabeling studies with GLIC and nAChR established that AziP*m* photoincorporates into a wide range of amino acid side chains, including aliphatic, aromatic, and nucleophilic, which demonstrates that it has the photoreactivity necessary to incorporate into binding sites of varying structure. The results also demonstrate, however, that in the nAChR propofol binds to some, but not all, of the sites binding AziP*m*.

Conclusions—Based upon [^{3}H]AziP*m* photolabeling of $\alpha1\beta3$ $GABA_ARs$, AziP*m* and propofol each bind to the β^+-α^-, α^+-β^-, and β^+-β^- intersubunit sites. Etomidate and *R*-*m*TFD-MPAB, anesthetics of complex structure, bind with >50-fold selectivity to the different classes of $GABA_AR$ intersubunit sites. In contrast, the modest differences in propofol affinity for the β^+-β^-, β^+-α^-, and α^+-β^- sites in the $\alpha1\beta3$ $GABA_AR$ establish that an anesthetic of such simple structure binds with little selectivity at each intersubunit site. Characterization of [^{3}H]AziP*m* photolabeling of $\alpha1\beta3\gamma2$ $GABA_AR$ (19) will provide further definition of the selectivities of propofol and other anesthetics for intersubunit sites in an $\alpha\beta\gamma$ $GABA_AR$ subtype representative of the heterotrimeric $GABA_ARs$ expressed most abundantly in the brain.

REFERENCES

1. Belelli, D., Lambert, J. J., Peters, J. A., Wafford, K., and Whiting, P. J. (1997) The interaction of the general anesthetic etomidate with the γ-aminobutyric acid type A receptor is influenced by a single amino acid. *Proc. Natl. Acad. Sci. U.S.A.* **94,** 11031–11036
2. Krasowski, M. D., Jenkins, A., Flood, P., Kung, A. Y., Hopfinger, A. J., and Harrison, N. L. (2001) General anesthetic potencies of a series of propofol analogs correlate with potency for potentiation of γ-aminobutyric acid (GABA) current at the GABA(A) receptor but not with lipid solubility. *J. Pharmacol. Exp. Ther.* **297,** 338–351
3. Jurd, R., Arras, M., Lambert, S., Drexler, B., Siegwart, R., Crestani, F., Zaugg, M., Vogt, K. E., Ledermann, B., Antkowiak, B., and Rudolph, U. (2003) General anesthetic actions *in vivo* strongly attenuated by a point mutation in the GABA(A) receptor β3 subunit. *FASEB J.* **17,** 250–252
4. Franks, N. P. (2008) General anaesthesia: from molecular targets to neuronal pathways of sleep and arousal. *Nat. Rev. Neurosci.* **9,** 370–386
5. Miller, P. S., and Smart, T. G. (2010) Binding, activation and modulation of Cys-loop receptors. *Trends Pharmacol. Sci.* **31,** 161–174
6. Sigel, E., and Steinmann, M. E. (2012) Structure, function, and modulation of $GABA_A$ receptors. *J. Biol. Chem.* **287,** 40224–40231
7. Krasowski, M. D., Nishikawa, K., Nikolaeva, N., Lin, A., and Harrison, N. L. (2001) Methionine 286 in transmembrane domain 3 of the GABA(A) receptor β subunit controls a binding cavity for propofol and other alkylphenol general anesthetics. *Neuropharmacology* **41,** 952–964
8. Bali, M., and Akabas, M. H. (2004) Defining the propofol-binding site location on the $GABA_A$ receptor. *Mol. Pharmacol.* **65,** 68–76
9. Richardson, J. E., Garcia, P. S., O'Toole, K. K., Derry, J. M., Bell, S. V., and Jenkins, A. (2007) A conserved tyrosine in the β2 subunit M4 segment is a determinant of γ-aminobutyric acid type A receptor sensitivity to propofol. *Anesthesiology* **107,** 412–418
10. Moraga-Cid, G., Yevenes, G. E., Schmalzing, G., Peoples, R. W., and Aguayo, L. G. (2011) A single phenylalanine residue in the main intracellular loop of α1 γ-aminobutyric acid type A and glycine receptors influences their sensitivity to propofol. *Anesthesiology* **115,** 464–473
11. Miller, P. S., and Aricescu, A. R. (2014) Crystal structure of a human $GABA_A$ receptor. *Nature* 10.1038/nature13293
12. Unwin, N. (2005) Refined structure of the nicotinic acetylcholine receptor at 4 Å resolution. *J. Mol. Biol.* **346,** 967–989
13. Hilf, R. J., and Dutzler, R. (2009) Structure of a potentially open state of a proton-activated pentameric ligand-gated ion channel. *Nature* **457,** 115–118
14. Zimmermann, I., and Dutzler, R. (2011) Ligand activation of the prokaryotic pentameric ligand-gated ion channel ELIC. *PLoS Biol.* **9,** e1001101
15. Hibbs, R. E., and Gouaux, E. (2011) Principles of activation and permeation in an anion-selective Cys-loop receptor. *Nature* **474,** 54–60
16. Chiara, D. C., Dostalova, Z., Jayakar, S. S., Zhou, X., Miller, K. W., and Cohen, J. B. (2012) Mapping general anesthetic-binding site(s) in human $\alpha1\beta3$ γ-aminobutyric acid type A receptors with [^{3}H]TDBzl-etomidate, a photoreactive etomidate analogue. *Biochemistry* **51,** 836–847
17. Bertaccini, E. J., Yoluk, O., Lindahl, E. R., and Trudell, J. R. (2013) Assessment of homology templates and an anesthetic-binding site within the γ-aminobutyric acid receptor. *Anesthesiology* **119,** 1087–1095
18. Li, G.-D., Chiara, D. C., Sawyer, G. W., Husain, S. S., Olsen, R. W., and Cohen, J. B. (2006) Identification of a $GABA_A$ receptor anesthetic-binding site at subunit interfaces by photolabeling with an etomidate analog. *J. Neurosci.* **26,** 11599–11605
19. Chiara, D. C., Jayakar, S. S., Zhou, X., Zhang, X., Savechenkov, P. Y., Bruzik, K. S., Miller, K. W., and Cohen, J. B. (2013) Specificity of intersubunit general anesthetic-binding sites in the transmembrane domain of the human $\alpha1\beta3\gamma2$ γ-aminobutyric acid type A ($GABA_A$) receptor. *J. Biol. Chem.* **288,** 19343–19357
20. Yip, G. M., Chen, Z. W., Edge, C. J., Smith, E. H., Dickinson, R., Hohenester, E., Townsend, R. R., Fuchs, K., Sieghart, W., Evers, A. S., and Franks, N. P. (2013) A propofol-binding site on mammalian $GABA_A$ receptors identified by photolabeling. *Nat. Chem. Biol.* **9,** 715–720
21. Hall, M. A., Xi, J., Lor, C., Dai, S., Pearce, R., Dailey, W. P., and Eckenhoff, R. G. (2010) *m*-Azipropofol (AziP*m*) a photoactive analogue of the intravenous general anesthetic propofol. *J. Med. Chem.* **53,** 5667–5675
22. Jayakar, S. S., Dailey, W. P., Eckenhoff, R. G., and Cohen, J. B. (2013) Identification of propofol-binding sites in a nicotinic acetylcholine receptor with a photoreactive propofol analog. *J. Biol. Chem.* **288,** 6178–6189
23. Nury, H., Van Renterghem, C., Weng, Y., Tran, A., Baaden, M., Dufresne, V., Changeux, J. P., Sonner, J. M., Delarue, M., and Corringer, P. J. (2011) X-ray structures of general anaesthetics bound to a pentameric ligand-gated ion channel. *Nature* **469,** 428–431
24. Chiara, D. C., Gill, J. F., Chen, Q., Tillman, T., Dailey, W. P., Eckenhoff, R. G., Xu, Y., Tang, P., and Cohen, J. (2014) Photoaffinity labeling the propofol-binding site in GLIC. *Biochemistry* **53,** 135–142
25. Savechenkov, P. Y., Zhang, X., Chiara, D. C., Stewart, D. S., Ge, R., Zhou, X., Raines, D. E., Cohen, J. B., Forman, S. A., Miller, K. W., and Bruzik, K. S. (2012) Allyl *m*-trifluoromethyldiazirine mephobarbital: an unusually potent enantioselective and photoreactive barbiturate general anesthetic. *J. Med. Chem.* **55,** 6554–6565
26. Husain, S. S., Ziebell, M. R., Ruesch, D., Hong, F., Arevalo, E., Kosterlitz, J. A., Olsen, R. W., Forman, S. A., Cohen, J. B., and Miller, K. W. (2003) 2-(3-methyl-3*H*-diaziren-3-yl) ethyl 1-(1-phenylethyl)-1*H*-imidazole-5-carboxylate: a derivative of the stereoselective general anesthetic etomidate for photolabeling ligand-gated ion channels. *J. Med. Chem.* **46,** 1257–1265
27. Dostalova, Z., Liu, A., Zhou, X., Farmer, S. L., Krenzel, E. S., Arevalo, E., Desai, R., Feinberg-Zadek, P. L., Davies, P. A., Yamodo, I. H., Forman, S. A., and Miller, K. W. (2010) High-level expression and purification of Cys-loop ligand-gated ion channels in a tetracycline-inducible stable mammalian cell line: GABA(A) and serotonin receptors. *Protein Sci.* **19,** 1728–1738
28. Scott, M. G., Crimmins, D. L., McCourt, D. W., Tarrand, J. J., Eyerman, M. C., and Nahm, M. H. (1988) A simple *in situ* cyanogen bromide cleavage method to obtain internal amino acid sequence of proteins electroblotted to polyvinyldifluoride membranes. *Biochem. Biophys. Res. Commun.* **155,** 1353–1359
29. Hamouda, A. K., Kimm, T., and Cohen, J. B. (2013) Physostigmine and

galanthamine bind in the presence of agonist at the canonical and noncanonical subunit Interfaces of a nicotinic acetylcholine receptor. *J. Neurosci.* **33,** 485–494
30. Crimmins, D. L., McCourt, D. W., Thoma, R. S., Scott, M. G., Macke, K., and Schwartz, B. D. (1990) *In situ* chemical cleavage of proteins immobilized to glass-fiber and polyvinylidene difluoride membranes: cleavage at tryptophan residues with 2-(2′-nitrophenylsulfenyl)-3-methyl-3′-bromoindolenine to obtain internal amino acid sequence. *Anal. Biochem.* **187,** 27–38
31. Brauer, A. W., Oman, C. L., and Margolies, M. N. (1984) Use of *o*-phthaldehyde to reduce background during automated Edman degradation. *Anal. Biochem.* **137,** 134–142
32. Middleton, R. E., and Cohen, J. B. (1991) Mapping of the acetylcholine-binding site of the nicotinic acetylcholine receptor: [^{3}H]nicotine as an agonist photoaffinity label. *Biochemistry* **30,** 6987–6997
33. Hamouda, A. K., Stewart, D. S., Husain, S. S., and Cohen, J. B. (2011) Multiple transmembrane-binding sites for *p*-trifluoromethyldiazirinyl-etomidate, a photoreactive *Torpedo* nicotinic acetylcholine receptor allosteric inhibitor. *J. Biol. Chem.* **286,** 20466–20477
34. Hamouda, A. K., Stewart, D. S., Chiara, D. C., Savechenkov, P. Y., Bruzik, K. S., and Cohen, J. B. (2014) Identifying barbiturate binding sites in a nicotinic acetylcholine receptor with [^{3}H]allyl *m*-trifluoromethyldiazirine mephobarbital, a photoreactive barbiturate. *Mol. Pharmacol.* **85,** 735–746
35. Blanton, M. P., and Cohen, J. B. (1994) Identifying the lipid-protein interface of the *Torpedo* nicotinic acetylcholine receptor: secondary structure implications. *Biochemistry* **33,** 2859–2872
36. Bali, M., and Akabas, M. H. (2012) Gating-induced conformational rearrangement of the γ-aminobutyric acid type A receptor β-α subunit interface in the membrane-spanning domain. *J. Biol. Chem.* **287,** 27762–27770
37. Bristow, D. R., and Martin, I. L. (1987) Solubilisation of the γ-aminobutyric acid/benzodiazepine receptor from rat cerebellum: optimal preservation of the modulatory responses by natural brain lipids. *J. Neurochem.* **49,** 1386–1393
38. Dunn, S. M., Martin, C. R., Agey, M. W., and Miyazaki, R. (1989) Functional reconstitution of the bovine brain $GABA_A$ receptor from solubilized components. *Biochemistry* **28,** 2545–2551
39. Sooksawate, T., and Simmonds, M. A. (2001) Influence of membrane cholesterol on modulation of the GABA(A) receptor by neuroactive steroids and other potentiators. *Br. J. Pharmacol.* **134,** 1303–1311
40. Hénin, J., Salari, R., Murlidaran, S., and Brannigan, G. (2014) A predicted-binding site for cholesterol on the $GABA_A$ receptor. *Biophys. J.* **106,** 1938–1949
41. Nirthanan, S., Garcia, G., 3rd., Chiara, D. C., Husain, S. S., and Cohen, J. B. (2008) Identification of-binding sites in the nicotinic acetylcholine receptor for TDBzl-etomidate, a photoreactive positive allosteric effector. *J. Biol. Chem.* **283,** 22051–22062
42. Pratt, M. B., Husain, S. S., Miller, K. W., and Cohen, J. B. (2000) Identification of sites of incorporation in the nicotinic acetylcholine receptor of a photoactivatable general anesthetic. *J. Biol. Chem.* **275,** 29441–29451
43. Bayley, H. (1983) *Photoregenerated Reagents in Biochemistry and Molecular Biology*, pp. 40–41, Elsevier, Amsterdam
44. Silva, Gd., and Bozzelli, J. W. (2007) Quantum chemical study of the thermal decomposition of *o*-quinone methide (6-methylene-2,4-cyclohexadien-1-one). *J. Phys. Chem. A* **111,** 7987–7994
45. Modica, E., Zanaletti, R., Freccero, M., and Mella, M. (2001) Alkylation of amino acids and glutathione in water by *o*-quinone methide: reactivity and selectivity. *J. Org. Chem.* **66,** 41–52
46. Cheng, T., Zhao, Y., Li, X., Lin, F., Xu, Y., Zhang, X., Li, Y., Wang, R., and Lai, L. (2007) Computation of octanol-water partition coefficients by guiding an additive model with knowledge. *J. Chem. Inf. Model.* **47,** 2140–2148